

Spotlighting the Simultaneous Formation of Coherent and Incoherent Dissipative Solitons in an Er-Doped Bidirectional Ultrafast Fiber Laser

Zhiqiang Wang^{1,2,3,*}, Qi Jiang,⁴ Nithyanandan Kanagaraj⁵, Benli Yu,^{1,2} and Zuxing Zhang^{4,†}


¹Information Materials and Intelligent Sensing Laboratory of Anhui Province, Anhui University, Hefei 230601, China

²Key Laboratory of Opto-Electronic Information Acquisition and Manipulation of Ministry of Education, Anhui University, Hefei 230601, China

³Aston Institute of Photonic Technologies, Aston University, Birmingham B4 7ET, United Kingdom

⁴College of Electronic and Optical Engineering, Nanjing University of Posts and Telecommunications, Nanjing 210023, China

⁵Department of Physics, Indian Institute of Technology Hyderabad, Kandi, Telangana 502285, India

 (Received 19 August 2022; revised 7 November 2022; accepted 6 December 2022; published 30 December 2022)

The emergence of localized structures originating from instabilities is of particular interest to scientists interested in exploring the rich nonlinear dynamics associated with complex dynamical systems. In the context of ultrafast lasers, the localized structures can be broadly divided into two categories: coherent structures of the dissipative soliton (DS) and incoherent structures such as the noiselike pulse (NLP). These two different types of structures have unique properties and applications and their physical origins are markedly different. Having both in a single fiber laser is an intriguing but challenging problem. Here we demonstrate the formation of the DS and NLP in a bidirectional ultrafast fiber laser and study their buildup dynamics from Q -switched instabilities. The clockwise light is a DS while the counterclockwise light is a NLP. The synchronized buildup dynamics of a DS or NLP from Q -switched instabilities provides vital evidence of the Q -switched instabilities as a universal indicator for the generation of localized structures in ultrafast lasers. The evenly spaced Q -switched spikes before the onset of a DS (NLP) exhibit intensity fluctuations, which is strikingly different than in the mode-locking regime in unidirectional oscillators, hence providing decisive evidence of the interaction between the counterpropagating light fields in the bidirectional lasers. The spectra cross-correlation and the histogram of the spectral intensity confirm the concurrent formation of a DS and NLP. Numerical simulations confirmed experimental observations. These findings help deepen understanding of the behavior of bidirectional ultrafast lasers and also demonstrate their potential as multifunctional ultrafast laser sources.

DOI: [10.1103/PhysRevApplied.18.064096](https://doi.org/10.1103/PhysRevApplied.18.064096)

I. INTRODUCTION

The mode synchronization or phase locking of longitudinal modes in a laser cavity produces ultrashort pulses due to the constructive interference between these modes. This technique is also popularly known as “mode locking.” Using this technique, one can build mode-locked ultrafast lasers that emit short pulses of the order of picoseconds or femtoseconds. Ultrafast lasers find many applications in optical communications, nonlinear optics, LIDIA, micro-machining, surgery, optical imaging, and spectroscopy [1]. The pulses circulating indefinitely in the laser cavity can maintain their shape on average, and hence are considered as coherent structures or “dissipative optical solitons.” Originally, the existence of optical solitons in

optical fibers was proposed in 1973 by Hasegawa and Tappert of AT&T Bell Labs [2]. They suggested that it was possible to achieve a stable coherent structure in an optical fiber through a delicate balance between self-phase modulation (SPM) and anomalous dispersion, which was identified as optical solitons. In the context of lasers, soliton mode locking is the technique that exploits the soliton effect to develop ultrafast soliton fiber lasers. Typically, a soliton fiber laser has fundamental performance constraints of limited pulse duration and energy [in the picojoule (pJ) regime] due to the soliton area theorem [2,3]. A dissipative soliton (DS) is an extension of traditional solitons [4–6] that can support a wide range of lasing states and possesses more functionalities to meet various applications. In optics, a DS is a localized electromagnetic field that is formed through energy exchange with the environment in the presence of SPM and dispersion or diffraction. The notion of a DS in ultrafast lasers offers a design concept for

*zhiqiangwang@ahu.edu.cn

†zxzhang@njupt.edu.cn

developing dissipative soliton lasers working in regimes such as the dispersion-managed solitons [7], similaritons [8,9], and a DS in the normal dispersion regime [5,10,11], yielding higher-energy chirped pulses (dozens of nanojoules) that can be externally compressed to the sub-10-fs level with compressors [12]. However, when the pulse gets too short, it becomes unstable in the cavity due to the excessive nonlinear phase shift. In some scenarios, the strong competition between the instability and the localizing effect leads to the generation of incoherent dissipative solitons, which are characterized by temporally localized pulse structures with chaotic pulse dynamics inside [13,14]. Such incoherent dissipative solitons in ultrafast lasers manifest in varied forms, for instance, soliton explosion [15,16], optical rogue waves [17], and noiselike pulses (NLP) [18,19], to mention a few.

The generation of structures, including coherent and incoherent dissipative solitons in ultrafast fiber lasers, is an intriguing subject in nonlinear optics. From the fundamental point of view, identifying the physical origin of these two markedly different regimes in ultrafast lasers helps to better understand the associated rich nonlinear dynamics in complex problems like fiber lasers and beyond. For instance, the concept of solitons applies to many fields spanning from optics [20] and plasma physics [21,22], to fluid dynamics [23] and Bose-Einstein condensations [24,25]. Likewise, the localized incoherent dissipative solitons, such as the NLP, have fundamental relevance in many fields and are often related to the generation of freak waves such as rogue waves, soliton explosion, etc. [17,19]. Consequently, understanding their kinetics would help predict extreme events in nature, such as freak ocean waves and extreme weather. From the viewpoint of applications, understanding the notion of a DS and NLP in ultrafast lasers is particularly important to advance laser performance. For instance, a DS fiber laser in a normal dispersion regime yields higher-energy ultrashort pulses on par with solid-state mode-locked lasers, in addition to their compact size, alignment-free, and low cost ownership [26]. On the other hand, the NLP in ultrafast fiber lasers produces a train of localized pulses with broad spectrum and higher-energy per pulse bunch and finds applications in the supercontinuum generation [27,28] and optical meteorology [29], to mention a few.

Interestingly, complex nonlinear systems like the ultrafast fiber laser can support infinite solutions and therefore operate in a wide range of stable states based on the choice of the system parameter. The DS and NLP are among the prominent stable structures one would typically encounter in a fiber laser system. The excessive nonlinear phase shift that accumulates as the pulse propagates in the cavity leads to instability and eventually results in a pulse split, thus paving the way for the multipulse operation. Under certain circumstances, these pulses can operate as a coherent bound state such as a soliton molecule [30–33] or

soliton molecular complexes [34–36]. In some instances, the interaction among pulses may also lead to NLP generation. It is worth noting that there are remarkable differences between the DS and NLP both in terms of physical origin as well as characteristics [18]. Therefore, having both the DS and NLP in tandem in a single ultrafast laser is extremely challenging and thus remains the principal objective of this work. One should note that addressing this challenge is not only a scientific curiosity but also helps to better understand the laser dynamics and thereby assist in the design of multifunctional ultrafast laser systems.

In this paper, we demonstrate the simultaneous formation of a DS and NLP from Q -switched instabilities in an Er-doped bidirectional ultrafast fiber laser in which clockwise (CW) light operates in a coherent DS regime while counterclockwise (CCW) light works in a partially mode-locking regime, namely the NLP regime. A bidirectional ultrafast fiber laser is a class of laser system that allows producing two sets of ultrashort pulse trains from counter-propagating directions in the cavity, which find wide applications, as a dual-comb source for a gyroscope [37,38] and dual-comb spectroscopy [39,40]. As CW and CCW light circulates the cavity in an opposite direction, it encounters intracavity components at different times; therefore, the time-dependent and power-dependent characteristics of the amplifier and the saturable absorber (SA) to the two propagating lights are different, which attribute to the cavity asymmetry. Recently, with the help of the real-time single-shot spectra measurement technique, namely, dispersive Fourier transform technology (DFT), Yu *et al.* [41] and Kudelin *et al.* [42] reported that the CW and CCW solitons in bidirectional lasers can evolve independently, exhibiting either similar buildup dynamics [41] or asynchronous buildup dynamics [42]. However, the counterpropagated light operating in different regimes in bidirectional ultrafast lasers is rarely exploited. Herein, we report the emergence of the DS and NLP at the same time from the counterpropagating directions in a bidirectional ultrafast fiber laser. The dynamics of their origin from Q -switched instabilities, the spectral cross-correlation, and the spectral rogue wave characteristics are analyzed, confirming the different regimes for CW and CCW light. Numerical simulations reproduce qualitatively similar dynamics.

II. EXPERIMENTAL SETUP

As shown in Fig. 1(a), the bidirectional ultrafast fiber laser is an erbium-doped fiber (EDF) ring laser consisting of a 0.7-m EDF and 4.9-m single-mode fiber (SMF). The EDF has a group velocity dispersion (GVD) of $76.9 \text{ ps}^2/\text{km}$ and a nonlinearity coefficient of $4 \text{ W}^{-1}/\text{km}$ at 1500 nm, which is bidirectionally pumped by two 980-nm pump laser diodes with a total maximum power of 1.3 W. A piece of the plug-and-play SA based on a single-wall carbon nanotube (SWCNT) is used to mode lock the laser. A

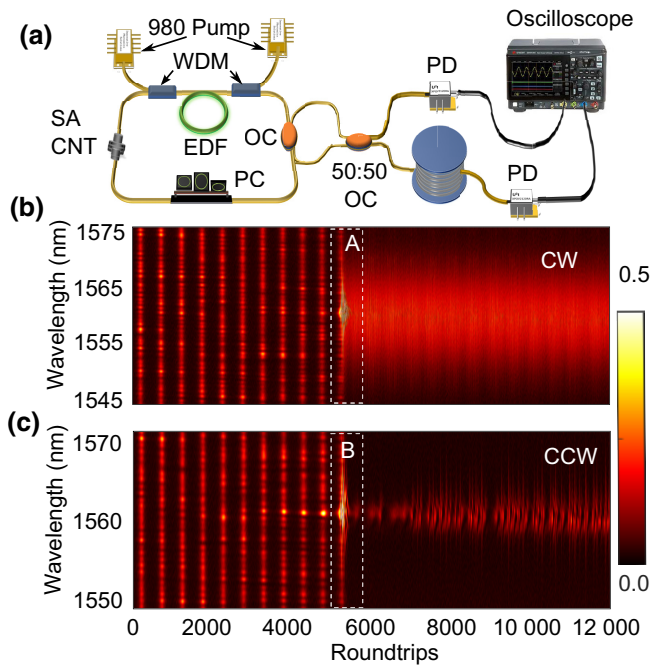


FIG. 1. (a) Schematic of the experimental setup of a bidirectional ultrafast fiber laser. WDM, wavelength-division multiplex; EDF, Er-doped fiber; OC, optical coupler; PC, polarization controller; SA CNT, carbon nanotube-based saturable absorber; DCF, dispersion compensation fiber; PD, photodetector. (b),(c) Real-time recorded experimental data of the buildup processes of CW and CCW light, respectively.

polarization controller (PC) is placed in the cavity to optimize the polarization state of the light. A four-port 50:50 coupler is used to extract the intracavity light for measurements. Since there is no optical isolator in the cavity, the intracavity light can propagate in both the CW and CCW directions. The SMF has a GVD of $-22.8 \text{ ps}^2/\text{km}$ and a nonlinearity coefficient of $1.3 \text{ W}^{-1}/\text{km}$ at 1500 nm . The total cavity length is 5.6 m , corresponding to a pulse repetition rate of 35.8 MHz . Consequently, the laser yields a total anomalous dispersion of -0.06 ps^2 , and hence works in the anomalous dispersion regime.

The output CW and CCW light from the cavity are combined through an optical coupler and sent to the DFT system for characterization. In principle, the DFT technology involves stretching the optical signal in the time domain with the help of dispersion devices like fibers, gratings, etc. [43]. Suppose that the total dispersion satisfies the far-field condition for diffraction; in that case, one can map the spectral intensity of the input signal onto the temporal profile of the output signal after the DFT system. This enables one to analyze the spectral evolution in real time at a repetition rate up to megahertz (typical for a fiber laser) using a digital oscilloscope. In our experiments, a 8.8-km -long dispersion compensation fiber (DCF) with a GVD of $56 \text{ ps}^2/\text{km}$ is used as the dispersion element. The

stretched signal is converted to electrical signals via a 15-GHz photodetector and connected to an 8-GHz real-time oscilloscope for visualization and data recording. The electrical spectrum resolution of our DFT is 0.1 nm , which is determined by the total GVD provided by the DCF and the bandwidth of the electronic system. To confirm the validity of the DFT measurement, the single-shot DFT spectrum is compared with the averaged spectrum obtained by an optical spectrum analyzer with a resolution of 0.02 nm [44].

III. EXPERIMENTAL RESULTS

In what follows, we study the formation and the dynamics of CW and CCW light in the bidirectional ultrafast laser based on the following attributes: (i) the buildup dynamics; (ii) the spectral similarity during the evolution; and (iii) the spectral rogue wave characterization.

A. Buildup dynamics

The laser is mode locked by using the SWCNT as the saturable absorber, while in the laser architecture containing polarization controllers, achieving stable mode locking of the DS usually requires a precise setting of the polarization controllers. In contrast, the incoherent NLP regime exists for a large range of polarization controller settings. The loose condition for NLP operation contrasts strongly with the strict and critical condition for mode locking of the DS, enabling us to fine tune the nonlinear transfer function of the polarization controller for both directions at the same time in the bidirectional laser through a small angle rotation of the polarization waveplates, which results in the generation of different operation regimes in different propagating directions. The whole procedure is well reproducible, though the fine details of the formed structures, such as pulse duration, precise temporal pulse location, and separation, can vary from one realization to the next. The threshold of mode locking in our bidirectional laser is about 100 mW . Therefore, we start at a pumping power of 100 mW and tune the polarization states to get the desired state, where the self-starting mode locking of the DS in the clockwise direction is accompanied with the generation of the NLP in the counterclockwise direction.

The buildup dynamics of CW and CCW light in the bidirectional fiber laser have been simultaneously recorded in real time using the DFT technique when the pump power ramps from zero to the threshold by suddenly switching on the pump current. Because of the limited record length of the oscilloscope, we set the time trigger to record only the evolving dynamics from Q -switched instabilities to the steady states in the laser. Figures 1(b) and 1(c) show the pseudocolor plots of the DFT spectral evolutions of CW and CCW light over 12000 roundtrips, clearly exhibiting the evenly spaced Q -switched pulses in the first 5300 roundtrips followed by different dynamics in the next

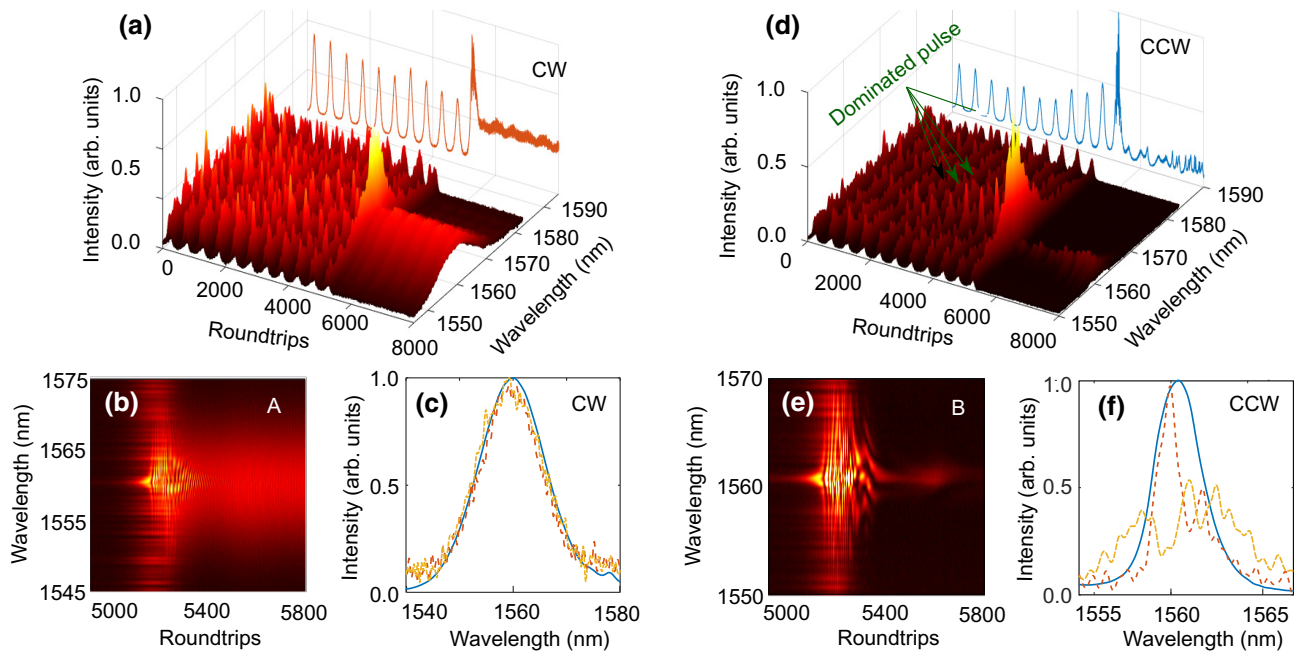


FIG. 2. Three-dimensional plots of the real-time recorded experimental data of the buildup process of (a)–(c) CW light and (d)–(f) CCW light, over 8000 roundtrips. The red curve in the X - O - Z plane in (a) shows the intensity of CW pulses evolving along with roundtrips. The cyan curve in the X - O - Z plane in (d) shows the intensity of CCW pulses evolving along with roundtrips. (b) Enlarged plot of the dynamics marked as A in the white dashed box in Fig. 1(b). (c) Averaged spectrum of CW light over 6000 roundtrips. Dashed red and yellow curves denote single-shot spectra at two different roundtrips. (e) Enlarged plot of the dynamics marked as B in the white dashed box in Fig. 1(c). (f) Averaged spectrum of CCW light over 6000 roundtrips. Dashed red and yellow curves denote single-shot spectra at two different roundtrips. Note the different coordinate ranges of the horizontal X axes in (c) and (f).

7000 roundtrips. Although CW and CCW light share the same gain fiber and SA in the cavity, the power-dependent characteristics of the amplifier and the SA transmittance force CW and CCW light to experience different gains and absorptions while propagating in the cavity. This is reflected by the asynchronous spectral intensity fluctuations of the Q -switched spikes in the range from the first roundtrip to the 5300th roundtrip shown in Figs. 2(a) and 2(d), suggesting interaction between the two counterpropagating light fields in the bidirectional laser configuration. This also leads to the different operation regimes of CW and CCW light in the end. In the range from roundtrip 8000 to 12 000, CW light maintains its broad spectral shape during propagation, thus featuring the generation of coherent solitons. The averaged spectrum of CW light over 6000 roundtrips shown in Fig. 2(c) also confirms the soliton operation. The dashed red and yellow curves are single-shot DFT spectra at two different roundtrips, which are almost the same as the averaged spectrum, further proving the generation of the DS in the CW direction. In contrast, CCW light exhibits chaotic and explosive behaviors as evident from the spectral intensity profile over roundtrips, indicating that the light structures in the CCW direction lose mutual coherence during the evolution. The single-shot DFT spectra at two different roundtrips better reflect the spectral explosive behavior. Unlike the

incoherent states such as white noise, CCW light is still localized and maintains its overall shape [see the smooth averaged spectrum of CCW light over 6000 roundtrips in Fig. 2(f)]. This intriguing yet complex pulse regime is the so-called *noiselike pulse*.

For better insight, the three-dimensional (3D) plots of the real-time recording of the spectrum evolutions are depicted in Figs. 2(a) and 2(d). The buildup phases of CW and CCW light have some global features in common. First of all, before the onset of mode locking, both CW and CCW light experience a Q -switching instability stage (from the first roundtrip to the 5000th roundtrip), although the spectral intensities for CW and CCW light are different due to gain competition and different transfer functions of the PC for the two directions. The red (cyan) curve in the X - O - Z plane in Fig. 2(a) [Fig. 2(d)] is the spectrum intensity of CW (CCW) light evolving along with roundtrips, showing evenly spaced spikes with a time interval of $13.95 \mu\text{s}$ (this corresponds to a repetition rate of 72 kHz, which is typically in the kilohertz level of the Q -switched regime). The constant time interval among these spikes provides satisfactory evidence of the Q -switching operation. Secondly, the spectral energy overshoot after the Q -switched operation and the sudden spectral broadening triggers the emergence of the DS (NLP) in the CW (CCW) direction. The energy overshoot in the evolution relates to

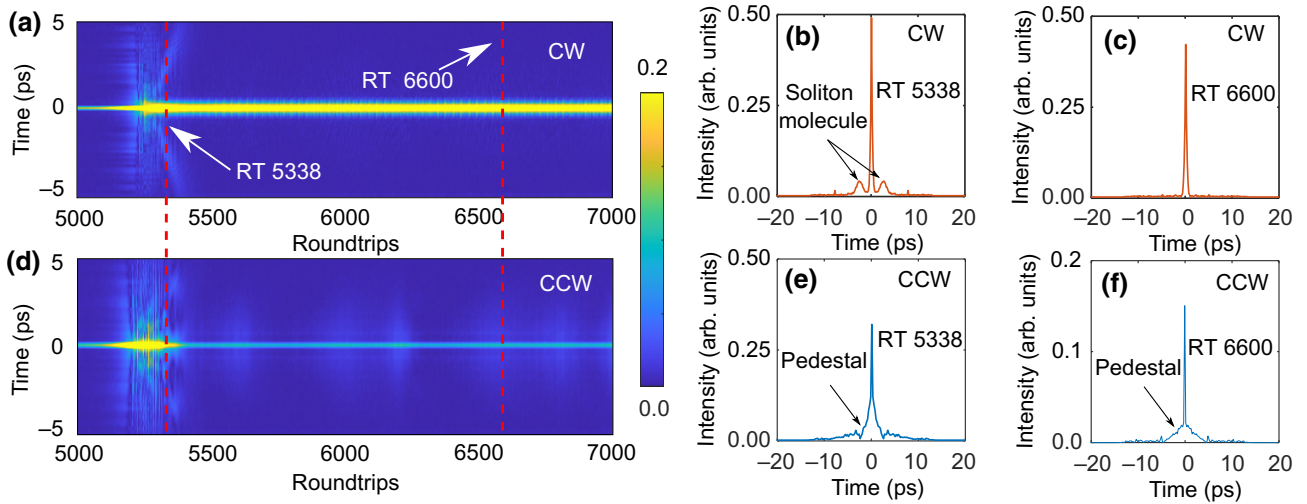


FIG. 3. Evolution of the pulse first-order AC trace over roundtrips via Fourier transforming the DFT spectra. (a) CW light. (d) CCW light. The vertical red lines cut at roundtrips (RTs) 5338 and 6600, and the corresponding AC traces are shown in (b)–(f). (b),(c) AC traces of CW light at roundtrips 5338 and 6600, respectively. (e),(f) AC traces of CCW light at roundtrips 5338 and 6600, respectively.

the gain relaxation oscillation [45] and is most often considered as an indication of the onset of coherent structures in ultrafast lasers [46].

Note that the peak intensity of the last spike of the normalized spectrum of CCW light is higher than the maximum peak intensity in the CW direction, suggesting that CCW light experiences a larger nonlinear phase shift that could attribute to the cavity asymmetry. The higher peak power contributes to the following buildup of the NLP in the CCW direction. An enlarged plot of the spectrum evolution in the roundtrips from 5000 to 5800 shows noticeable beating dynamics on the road towards the soliton states in the CW direction. In contrast, for CCW light, apparent interference spectral fringes are observed, shown in Fig. 2(e). In the CW direction, a dominant pulse survives in the competition with many precursor pulses, and at the same time beats with small pulses, giving the beating pattern exhibited in Fig. 2(b). For CCW light, the relatively higher spectral intensity induces the spectral collapse, accompanied by the pulse split and interactions, leading to the apparent interference spectrum, presented in Fig. 2(e). The pulse splitting can also be confirmed by the sudden drop in its spectral intensity to nearly zero [cyan curve in Fig. 2(d)]. These two scenarios have been reproduced and confirmed by numerical simulations (see Sec. IV). We must emphasize that both the spectral beating and interference could be involved in the buildup dynamics but which dominates the evolution depends critically on the pulse properties and system parameters.

According to the Wiener-Khinchin theorem [47–49], taking the Fourier transform of the spectrum intensity yields the first-order autocorrelation (AC) trace. This method has been successfully used to analyze the internal dynamics of soliton molecules and transient dynamics

of dissipative structures in various dissipative systems [31,34]. To characterize the different dynamics of CW and CCW light in the transient stage before the onset of the steady operation, we depict the evolutions of the AC traces of CW and CCW light in a range of roundtrips from 5000 to 7000 in Figs. 3(a) and 3(d). In accordance with the spectral dynamics in Figs. 2(b) and 2(e), the AC traces in the transient stage exhibit complex structures from roundtrip 5200 to 5400, evidencing the emergence of multipulse and irregular interactions among pulses, which leads to the beating pattern shown in Fig. 2(d) and the interference pattern observed in Fig. 2(e). The beating dynamics and spectral interference of CW light occur in a very short time scale, less than 100 roundtrips, and soon after that, one dominant pulse evolves into a stable soliton accompanied by the annihilation of small pulses. The symmetric side lobes located on the AC trace at roundtrip 5338 shown in Fig. 3(b) confirm the formation of multipulses in the buildup process. Figure 3(c) is a single shot of the AC trace of CW light at roundtrip 6600 with a clear single peak, confirming the soliton operation. For CCW light, the apparent pedestal that exists in the whole evolving process provides evidence of NLP operation [see the AC traces in Figs. 3(e) and 3(f)].

B. Spectra cross-correlation map

The cross-correlation (CC) of the spectrum is an effective parameter to estimate the spectral similarity at different roundtrips. Calculation of the CC maps of CW and CCW light in the buildup phase enables us to get more insights into the buildup dynamics of CW and CCW structures. The CC can be calculated using the formula

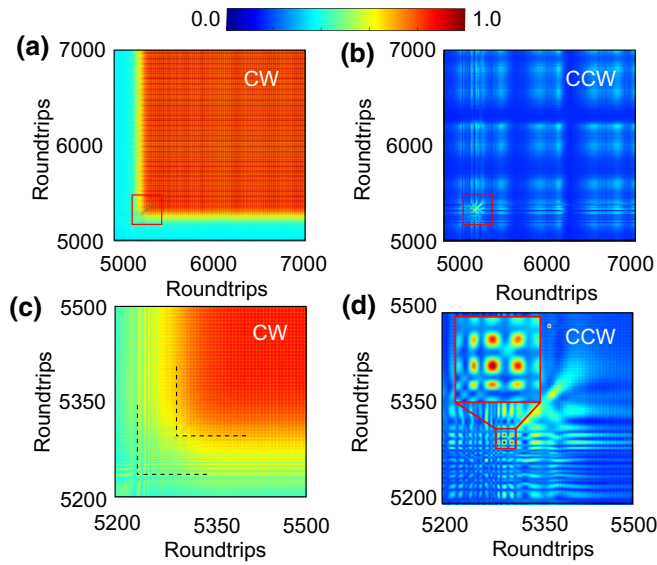


FIG. 4. Spectral CC maps of (a) CW light and (b) CCW light. (c),(d) Enlarged versions of the maps within a range from roundtrip 5200 to 5500. The inset in (d) is to show the periodic appearance of the higher intensity dots from roundtrip 5280 to 5320 corresponding to the formation of coherent structures of multipulses.

[50]

$$CC_{n,n+1}(\lambda) = \frac{[\int I_n(\lambda)I_{n+1}(\lambda)d\lambda]^2}{\int [I_n(\lambda)]^2 d\lambda \int [I_{n+1}(\lambda)]^2 d\lambda}, \quad (1)$$

where $I_n(\lambda)$ is the spectral intensity profile at roundtrip n . Starting from the 5000th roundtrip, as shown in Fig. 4(a), CW light evolves from the noise field with lower coherence and soon enters the soliton buildup phase, accompanied by an increase in the spectral coherence, which is revealed by the color transitions from green at roundtrip 5000 to yellow at roundtrip 5300. In Fig. 4(c), an enlarged plot of the rectangular area marked by the red box in Fig. 4(a) shows that it takes almost 100 roundtrips (2.8 μ s) for CW light to evolve into stable DSs. Clear periodic enhancement of the spectral coherence [periodic yellow lines in Fig. 4(c)] in the range from roundtrip 5250 to 5300 corresponds to the beating pattern shown in Fig. 2(b). After roundtrip 5300, the CC values tend to be a constant of 1, which is confirmed by the homogeneous color maps shown in Figs. 4(a) and 4(c). This ensures the high similarity between the consecutive spectrum and the stable mode locking of solitons of CW light.

In strong contrast, the CC map of CCW light is quite different, due to the different operating regimes. In general, the overall value of CC shown in Figs. 4(b) and 4(d) has a relatively lower value (less than 0.5), compared to the CC map of CW light. The periodic pattern shown in Fig. 4(b) suggests the recurrence of the low spectral coherence in the NLP buildup phase (roundtrip range from 5200

to 7000), which corresponds to the quasiperiodic soliton explosion shown in Fig. 1(c). Note that in Fig. 4(d) we still see the periodic enhancement of the spectral coherence before and after the energy overshoot from roundtrip 5200 to 5400, strengthening the fact that the energy overshoot is universal, serving as an indication for the onset of incoherent NLP structures in ultrafast lasers. The periodic higher intensity dots with CC value close to 1 in a narrow range around roundtrip 5300 (see the inset: from roundtrip of 5280 to 5320) in Fig. 4(d) correspond to the coherent multipulses formation and interactions. It is also interesting to note that only in a range from roundtrip 5320 to 5450 the map shows higher CC values on the diagonal, which further confirms the lack of coherence between the spectra at different roundtrips.

C. Spectral rogue wave characterization

The formation of the NLP in ultrafast fiber lasers seems paradoxical, as it manifests as a localized temporal structure with strong pulse-pulse instability. Typically, the NLP encompasses several subpicosecond solitonlike pulses of different amplitudes exhibiting strong interaction dynamics while lacking the mutual phase coherence from roundtrip to roundtrip. The pulses hence move with different velocities depending on their amplitudes and interact with each other, leading to the generation of optical rogue waves [17,51].

Rogue waves (RWs) are extreme waves that typically appear in complex nonlinear systems under delicate operating conditions. They appear unexpectedly with huge amplitude and disappear without any trace. In an optical context, previous literature demonstrates the formation of a RW in a supercontinuum system in which the RW was generated near the threshold of the soliton fission. Extremely large amplitude waves were observed while evaluating the statistical behaviors of the spectral intensity measured using DFT [52]. The criteria to quantify RWs is the generation of waves whose height is more than twice the significant wave height (SWH), which is defined as the highest third of waves in the record.

A statistic of the spectral intensity over thousands of roundtrips enables us to distinguish the different regimes for CW and CCW light in the bidirectional ultrafast fiber laser. Figure 5(c) shows the statistic of the maximum spectral peak height of the single-shot spectrum of CW light shown in Fig. 5(a). As CW light operates in a stable soliton regime, the height of the spectra over 4000 roundtrips concentrates in a narrow range with a mean value close to 1. The single peak AC trace without a pedestal, as shown in Fig. 5(e), confirms the soliton generation. In contrast, the light in the CCW direction experiences irregular spectral explosion over roundtrips, as shown in Fig. 5(b), and the statistics of the spectral peak reveal the generation of waves with a more prominent peak twice that of the I_{SWH}

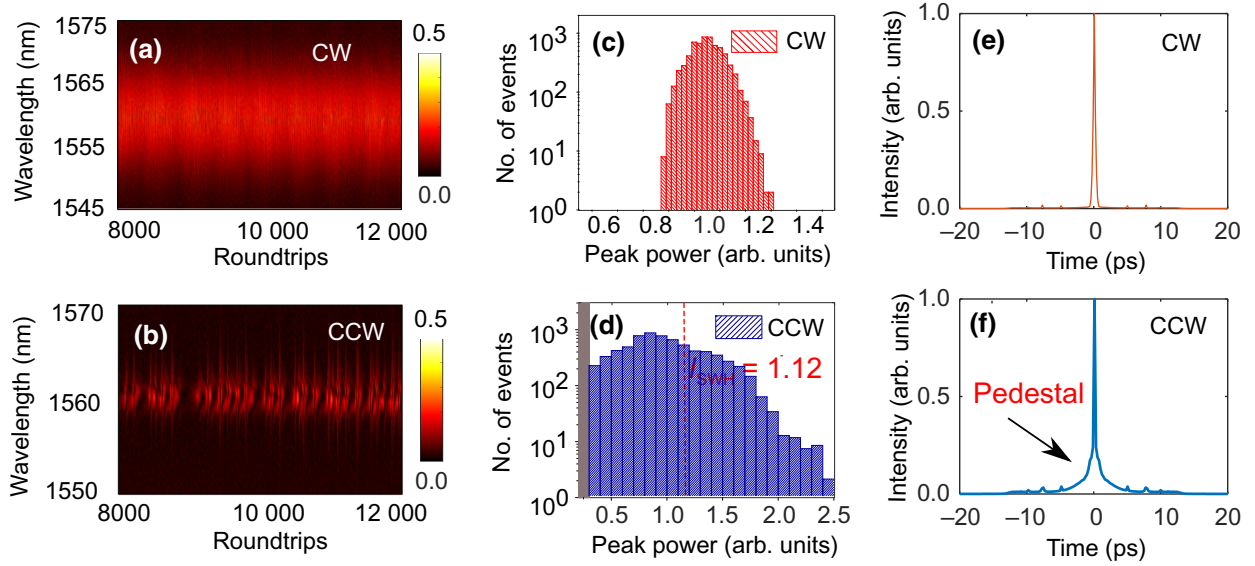


FIG. 5. Spectral rogue wave characterization. (a),(b) Single-shot DFT spectrum evolutions of CW and CCW light, respectively, in a range from roundtrip 8000 to roundtrip 12 000. (c),(d) Histograms showing the distributions of the optical intensities of CW and CCW light, respectively. The vertical red line in (d) indicates the SWH. (e),(f) Averaged AC traces of CW and CCW light, respectively.

[see Fig. 5(d)], thus confirming the optical rogue wave generation in the CCW direction. The notable pedestal on the base of the averaged AC trace shown in Fig. 5(f) is a typical manifestation of NLP operation.

IV. SIMULATION

A. Simulation model

To corroborate the experimental observations, we carry out simulations based on a lumped scalar model for the laser configuration and parameters. A schematic diagram of the simulation model is presented in Fig. 6. The various optical components forming the cavity are concatenated in the same fashion with the help of appropriate transfer functions and equations. The details of the fiber length and parameters are given in Table I. The pulse propagating in fibers is modeled using a nonlinear Schrödinger equation as follows:

$$\frac{\partial A}{\partial z} = \frac{g - \alpha}{2} A - i \frac{\beta_2}{2} \frac{\partial^2 A}{\partial t^2} + i \gamma |A|^2 A + \frac{g}{2\Omega_g^2} \frac{\partial^2 A}{\partial t^2}. \quad (2)$$

Here A is the slowly varying envelope, g and α are respectively the fiber gain and loss, β_2 is the group velocity dispersion, γ is the nonlinearity coefficient, Ω_g is the gain bandwidth, and P_{sat} is the saturation power corresponding to the active fiber. The gain g in the fiber is described using the formula [40]

$$g = g_0 \exp\left(-\frac{P_{\text{CW}} + P_{\text{CCW}}}{P_{\text{sat}}}\right), \quad (3)$$

where g_0 is the small-signal gain of the active fiber, and $P_{\text{CW/CCW}}$ are the instantaneous powers of CW and CCW light. The SWCNT-based SA is modeled by a standard SA function given by

$$T_{\text{SA}} = 1 - a_0 - \frac{a_m}{1 + (E_{\text{CW}} + E_{\text{CCW}})/E_{\text{sat}}}, \quad (4)$$

where a_0 is the linear loss of the SA, a_m is the modulation depth, $E_{\text{CW/CCW}}$ are the instantaneous pulse energies of CW and CCW light, and E_{sat} is the saturation energy of the SA. Considering the asymmetry of the laser cavity, the PC in the experiments is also considered and modeled by using the transfer function

$$T_{\text{PC}} = \begin{pmatrix} \cos\theta_{1,2} & -\sin\theta_{1,2} \\ \sin\theta_{1,2} & \cos\theta_{1,2} \end{pmatrix} \begin{pmatrix} e^{-i\phi_{1,2}/2} & 0 \\ 0 & e^{i\phi_{1,2}/2} \end{pmatrix} \times \begin{pmatrix} \cos\theta_{1,2} & \sin\theta_{1,2} \\ -\sin\theta_{1,2} & \cos\theta_{1,2} \end{pmatrix}, \quad (5)$$

where θ represents the angle between the coordinates of the PC and one of the polarization states of CW (CCW) light, and ϕ is the phase difference between the orthogonal polarization components induced by the PC. CW and CCW light passes through the PC in reverse order in simulations.

The time window for the simulation is set to 100 ps with 2^{11} data points. Equation (2) is solved by using the split-step Fourier method with white noise as the initial field. The linear terms are solved in the frequency domain, while the nonlinear terms are integrated in the time domain using the RK4. Because of a lack of access to the exact SA parameters, the steady-state solutions of

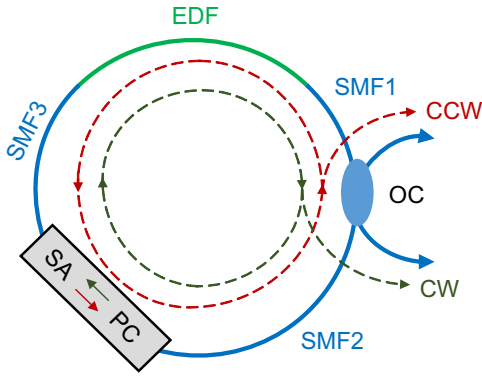


FIG. 6. Schematic diagram of the simulation model. EDF, erbium-doped fiber; SMF, single-mode fiber; OC, four-port 50:50 optical coupler; SA, saturable absorber; PC, three-paddle polarization controller.

CW and CCW light are obtained after several trials with different parameter sets.

B. Simulation results

Figure 7 shows the simulation results using the following parameters: $g_0 = 8.5 \text{ m}^{-1}$, $\Omega_g = 40 \text{ nm}$, $a_0 = 0.5$, $a_m = 0.1$, $E_{\text{sat}} = 300 \text{ pJ}$, $P_{\text{sat}} = 8 \text{ W}$, $\theta_1 = 0.1\pi$, $\theta_2 = 0.65\pi$, $\phi_1 = 0.2\pi$, and $\phi_2 = 0.4\pi$.

Figure 7(a) shows the spectrum evolution of CW light over 300 roundtrips, demonstrating the buildup of a stable soliton state from the initial noise field through different phases including the modulation instability (MI) induced multipulse formation, spectral beating, pulse annihilation, and single soliton formation. The spectrum at roundtrip 300 with symmetric side lobes (Kelly sidebands) shown in Fig. 7(b) and the corresponding clear AC trace shown in Fig. 7(c) confirm the stable mode-locking operation of a single soliton in the CW direction.

In contrast, CCW light operates in the NLP regime for the same parameters. An apparent multipulse state is observed after the MI in the first 20 roundtrips, which can be seen from the interference spectrum shown in Fig. 7(d). Along with the evolution in the following 20 roundtrips, the solitons repel each other, leading to a decrease in the period of the interference spectrum. The strength of the interaction among the solitons depends on their amplitude, soliton separations, and relative phase. Typically, when the

soliton separation is larger than several orders of magnitude of its pulse width, the interaction between two solitons becomes very weak. Therefore, solitons that break up from the original multipulses will interact with each other, leading to the generation of a partially coherent spectrum, as shown in Fig. 7(d). Figure 7(e) shows the single-shot spectrum with delicate structures inside (black dashed curve) and a smooth spectrum averaged over 200 roundtrips (cyan curve). An averaged AC trace over 200 roundtrips is also shown in Fig. 7(f), featuring a narrow coherent spike sitting on a broad pedestal, which is a signature of the NLP regime.

We note that our numerical model fails to reproduce the initial phase of Q -switched instabilities as we observed in the experimental recording in the first 5300 roundtrips. It can be attributed to the simple lumped model that we use in the simulations. On the one hand, the finite time window of 100 ps in simulations only represents a small fraction of the cavity roundtrip time, resulting in difficulty simulating the dynamical evolution of long pulses such as nanosecond-long Q -switched chaotic pulses distributed along the whole cavity. On the other hand, the model does not consider the gain evolution along the fiber and the gain competition as well as the interaction between the CW and CCW light fields in the bidirectional ultrafast laser. A more precise model considering all relevant physical effects is desired for simulating bidirectional ultrafast lasers in the future, though the current simple model is valid for corroborating distinct regimes in the experimental observations.

V. DISCUSSION

Courtesy of the real-time shot-to-shot spectral measurements with the help of DFT technology, we precisely resolve the buildup of pulses from the counterpropagating directions in an Er-doped bidirectional ultrafast laser. The simultaneous generation of NLP and soliton components in a ring fiber configuration had previously been reported by Bracamontes Rodríguez *et al.* [53], wherein the soliton components are multipulses presented in a form of soliton rain due to the excessive gain that is required by the NLP operation in the cavity. The multipulse feature prevents such a type of dual operational laser for practical applications. Characteristically, we demonstrate the simultaneous formation and the coexistence of the coherent structure of the DS and the incoherent NLP in a single ultrafast fiber laser. In the CW direction, the DS works in a steady state at a fundamental repetition rate, namely only one pulse circulating in the cavity per roundtrip. This feature enables our dual-operational laser to be used as a multifunctional laser source for many practical applications. Our experimental results and the simulations circumstantiate that both the DS and NLP originate from the intracavity Q -switched instabilities, showing similar buildup dynamics of solitons as in the case of conventional unidirectional mode-locked

TABLE I. Fiber parameters.

	β_2 (ps ² /km)	β_3 (ps ³ /km)	γ (W ⁻¹ /km)	L (m)
EDF	67.2	0.16×10^{-3}	4	0.7
SMF1	-22.8	0.088×10^{-3}	1.3	0.4
SMF2				2.3
SMF3				2.2

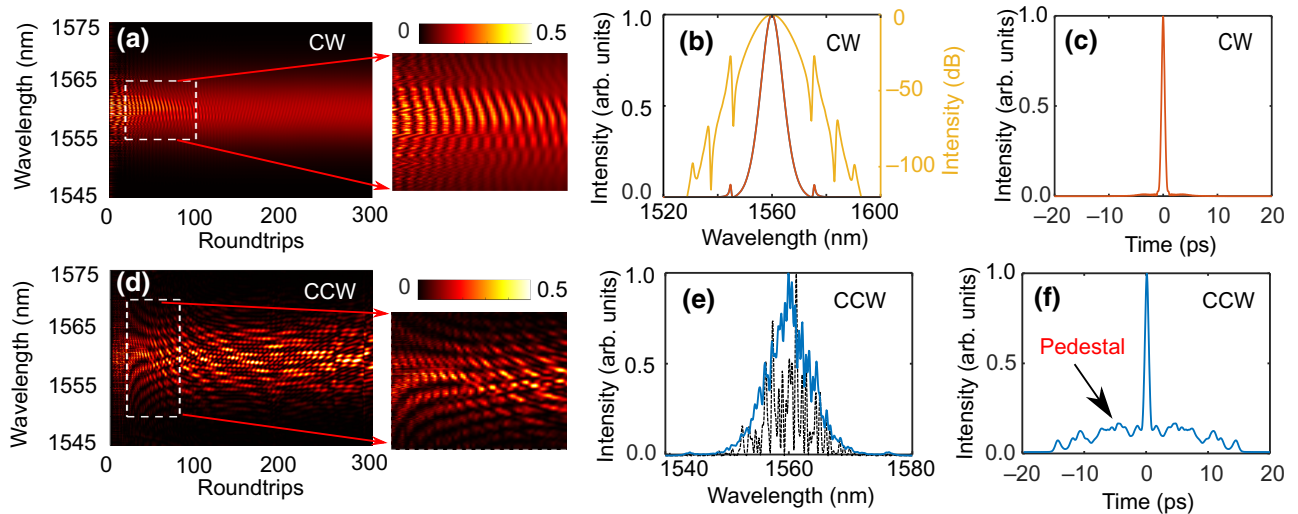


FIG. 7. Simulation results. Spectrum evolutions of (a) CW light and (b) CCW light along with roundtrips. The initial condition is a white noise field. (b) Single-shot spectrum of the CW soliton spectrum on a linear scale (red curve) and log scale (yellow curve). (c) Autocorrelation trace of CW pulses. (e) Single-shot spectrum (black dashed curve) and averaged spectrum (cyan solid curve) of CCW light over the last 200 roundtrips. (f) Averaged autocorrelation trace of CCW pulses showing NLP operation.

fiber laser systems [46,54,55]. Different stages, including Q switching, multipulse formation, spectral beating, pulse annihilation, and DS and NLP formation, are observed in the buildup process. Energy overshoot typical to the Q -switching instabilities is also noticed before the onset of the DS or NLP, which enables us to consider it a universal indicator for the generation of temporally localized structures in ultrafast lasers. Depending on the pulse properties, such as the pulse intensity and its peak power, the intracavity CW or CCW field in the bidirectional laser evolves into different stationary states at the end after the energy overshoot. In our experiments, the final state in the CW direction is a fully coherent state of the DS, which is confirmed by the spectral CC map and the statistics of the spectral intensity over thousands of roundtrips. In sharp contrast to CW light, CCW light operates in a partially mode-locked state, specifically in the NLP regime. The fluctuations of the spectral intensity, the low CC value, the nonperiodic spectra explosion, and the generation of the extreme waves over roundtrips provide satisfactory evidence of the NLP regime.

The rich dynamics of CW and CCW light in the underlined Er-doped ultrafast fiber laser suggest that the bidirectional lasers are ideal choices for investigating complex nonlinear soliton dynamics. The gain competition in the active fiber and the interaction between the counterpropagating light field in the intracavity components, for instance, the collision in the SA, are responsible for these complex dynamics [42,56,57]. When compared to the dynamics of mode locking of solitons from Q -switching instabilities in unidirectional ultrafast lasers [55], we observe in our experiments the obvious fluctuations in the spectral intensities of evenly spaced Q -switched spikes

[see Figs. 2(a) and 2(d)], reflecting the interaction between the counterpropagating light field over roundtrips during the Q -switching stage. Therefore, the interaction between the counterpropagating light field provides another degree of freedom to simultaneously access different operational regimes in one laser, thus making the bidirectional laser suitable for studying complex soliton interactions.

Contemporary to the previous reports [40,44,58,59], our works demonstrate the intriguing real-time dynamics of dual DS and NLP operation in bidirectional ultrafast fiber lasers experimentally and numerically, showing the DS operation in the CW direction and NLP operation in the CCW direction. These findings pave the way for the realization of multifunctional ultrafast lasers. It should be noted that the counterpropagating solitons in microresonators have been a topic of broad interest and successfully reported in Refs. [60,61]. Considering the diverse regimes that exist in microresonators, such as Turing patterns, chaotic pulses, breathers, and Kerr solitons [62,63], we expect the simultaneous generation of different structures from the counterpropagation directions in a single microresonator on chip. Indeed, this is a major breakthrough and could pave the way for the realization of compact multifunctional sources for applications in spectroscopy, ranging system, and optical imaging.

VI. CONCLUSION

In conclusion, we have demonstrated the simultaneous generation of the DS and NLP from the counterpropagating directions in an Er-doped bidirectional ultrafast fiber laser. The buildup dynamics of the DS and NLP from Q -switched instabilities in the cavity are recorded and

analyzed from the perspective of spectrum evolution, spectral cross-correlations, and the statistical interpretation of the spectral intensity over roundtrips. Experimental results reveal the synchronous Q -switching dynamics and the formation of distinct final states of the counterpropagating light through different stages. In the CCW direction the laser operates in the NLP regime, featuring the generation of optical rogue waves, while in the CW direction the laser works in a stable soliton regime. The interplay between the counterpropagating light fields plays an important role in these complex dynamics. Our findings provide decisive experimental evidence of the simultaneous generation of the DS and NLP in one ultrafast fiber laser. The present study would add a deeper understanding of the emergence of coherent and incoherent structures in nonlinear systems and thus pave the way for applications of bidirectional ultrafast lasers as multifunctional ultrafast laser sources.

ACKNOWLEDGMENTS

The authors acknowledge support from the National Natural Science Foundation of China (Grants No. 91950105 and No. 62175116), the European Commission Marie Curie Individual Fellowship (Grant No. 891017), the Jiangsu Shuangchuang Outstanding Doctor Talents Support Program (Grant No. CZ1060619002), and the Natural Science Foundation of Jiangsu Province (Grant No. BK20180742)

-
- [1] M. E. Fermann, A. Galvanauskas, and G. Sucha, *Ultrafast Lasers: Technology and Applications*, Vol. 80 (CRC Press, Boca Raton, 2002).
- [2] A. Hasegawa and F. Tappert, Transmission of stationary nonlinear optical pulses in dispersive dielectric fibers. I. Anomalous dispersion, *Appl. Phys. Lett.* **23**, 142 (1973).
- [3] S. L. McCall and E. L. Hahn, Self-Induced Transparency by Pulsed Coherent Light, *Phys. Rev. Lett.* **18**, 908 (1967).
- [4] E. Vanin, A. Korytin, A. Sergeev, D. Anderson, M. Lisak, and L. Vázquez, Dissipative optical solitons, *Phys. Rev. A* **49**, 2806 (1994).
- [5] P. Grelu and N. Akhmediev, Dissipative solitons for mode-locked lasers, *Nat. Photon.* **6**, 84 (2012).
- [6] N. Akhmediev and A. Ankiewicz, *Dissipative Solitons: from Optics to Biology and Medicine*, Vol. 751 (Springer, Berlin Heidelberg, 2008).
- [7] S. K. Turitsyn, B. G. Bale, and M. P. Fedoruk, Dispersion-managed solitons in fibre systems and lasers, *Phys. Rep.* **521**, 135 (2012).
- [8] F. Ilday, J. Buckley, W. Clark, and F. Wise, Self-Similar Evolution of Parabolic Pulses in a Laser, *Phys. Rev. Lett.* **92**, 213902 (2004).
- [9] B. Oktem, C. Ülgüdür, and F. Ö. Ilday, Soliton-similariton fibre laser, *Nat. Photon.* **4**, 307 (2010).
- [10] A. Chong, J. Buckley, W. Renninger, and F. Wise, All-normal-dispersion femtosecond fiber laser, *Opt. Express* **14**, 10095 (2006).
- [11] L. Zhao, D. Tang, T. Cheng, and C. Lu, Gain-guided solitons in dispersion-managed fiber lasers with large net cavity dispersion, *Opt. Lett.* **31**, 2957 (2006).
- [12] D. H. Sutter, G. Steinmeyer, L. Gallmann, N. Matuschek, F. Morier-Genoud, U. Keller, V. Scheuer, G. Angelow, and T. Tschudi, Semiconductor saturable-absorber mirror-assisted Kerr-lens mode-locked Ti:sapphire laser producing pulses in the two-cycle regime, *Opt. Lett.* **24**, 631 (1999).
- [13] K. Krupa, K. Nithyanandan, and P. Grelu, Vector dynamics of incoherent dissipative optical solitons, *Optica* **4**, 1239 (2017).
- [14] M. Horowitz, Y. Barad, and Y. Silberberg, Noiselike pulses with a broadband spectrum generated from an erbium-doped fiber laser, *Opt. Lett.* **22**, 799 (1997).
- [15] S. T. Cundiff, J. M. Soto-Crespo, and N. Akhmediev, Experimental Evidence for Soliton Explosions, *Phys. Rev. Lett.* **88**, 073903 (2002).
- [16] A. F. Runge, N. G. Broderick, and M. Erkintalo, Observation of soliton explosions in a passively mode-locked fiber laser, *Optica* **2**, 36 (2015).
- [17] C. Lecaplain, P. Grelu, J. Soto-Crespo, and N. Akhmediev, Dissipative Rogue Waves Generated by Chaotic Pulse Bunching in a Mode-Locked Laser, *Phys. Rev. Lett.* **108**, 233901 (2012).
- [18] Z. Wang, K. Nithyanandan, A. Coillet, P. Tchofo-Dinda, and P. Grelu, Buildup of incoherent dissipative solitons in ultrafast fiber lasers, *Phys. Rev. Res.* **2**, 013101 (2020).
- [19] C. Lecaplain and P. Grelu, Rogue waves among noiselike-pulse laser emission: An experimental investigation, *Phys. Rev. A* **90**, 013805 (2014).
- [20] Y. S. Kivshar and G. P. Agrawal, *Optical Solitons: from Fibers to Photonic Crystals* (Academic press, San Diego, 2003).
- [21] H. Washimi and T. Taniuti, Propagation of Ion-Acoustic Solitary Waves of Small Amplitude, *Phys. Rev. Lett.* **17**, 996 (1966).
- [22] H. Ikezi, R. Taylor, and D. Baker, Formation and Interaction of Ion-Acoustic Solitons, *Phys. Rev. Lett.* **25**, 11 (1970).
- [23] J. Wu, R. Keolian, and I. Rudnick, Observation of a Non-propagating Hydrodynamic Soliton, *Phys. Rev. Lett.* **52**, 1421 (1984).
- [24] S. Burger, K. Bongs, S. Dettmer, W. Ertmer, K. Sengstock, A. Sanpera, G. V. Shlyapnikov, and M. Lewenstein, Dark Solitons in Bose-Einstein Condensates, *Phys. Rev. Lett.* **83**, 5198 (1999).
- [25] L. Khaykovich, F. Schreck, G. Ferrari, T. Bourdel, J. Cubizolles, L. D. Carr, Y. Castin, and C. Salomon, Formation of a matter-wave bright soliton, *Science* **296**, 1290 (2002).
- [26] F. W. Wise, A. Chong, and W. H. Renninger, High-energy femtosecond fiber lasers based on pulse propagation at normal dispersion, *Laser Photon. Rev.* **2**, 58 (2008).
- [27] J. Hernandez-Garcia, O. Pottiez, and J. Estudillo-Ayala, Supercontinuum generation in a standard fiber pumped by noise-like pulses from a figure-eight fiber laser, *Laser Phys.* **22**, 221 (2012).
- [28] A. Zaytsev, C.-H. Lin, Y.-J. You, C.-C. Chung, C.-L. Wang, and C.-L. Pan, Supercontinuum generation by noise-like pulses transmitted through normally dispersive standard single-mode fibers, *Opt. Express* **21**, 16056 (2013).

- [29] S. Keren and M. Horowitz, Interrogation of fiber gratings by use of low-coherence spectral interferometry of noiselike pulses, *Opt. Lett.* **26**, 328 (2001).
- [30] K. Krupa, K. Nithyanandan, U. Andral, P. Tchofo-Dinda, and P. Grelu, Real-Time Observation of Internal Motion within Ultrafast Dissipative Optical Soliton Molecules, *Phys. Rev. Lett.* **118**, 243901 (2017).
- [31] G. Herink, F. Kurtz, B. Jalali, D. R. Solli, and C. Ropers, Real-time spectral interferometry probes the internal dynamics of femtosecond soliton molecules, *Science* **356**, 50 (2017).
- [32] X. Liu, X. Yao, and Y. Cui, Real-Time Observation of the Buildup of Soliton Molecules, *Phys. Rev. Lett.* **121**, 023905 (2018).
- [33] J. Peng and H. Zeng, Build-up of dissipative optical soliton molecules via diverse soliton interactions, *Laser Photon. Rev.* **12**, 1800009 (2018).
- [34] Z. Wang, K. Nithyanandan, A. Coillet, P. Tchofo-Dinda, and P. Grelu, Optical soliton molecular complexes in a passively mode-locked fibre laser, *Nat. Commun.* **10**, 1 (2019).
- [35] W. He, M. Pang, D.-H. Yeh, J. Huang, C. Menyuk, and P. S. J. Russell, Formation of optical supramolecular structures in a fibre laser by tailoring long-range soliton interactions, *Nat. Commun.* **10**, 1 (2019).
- [36] W. He, M. Pang, D.-H. Yeh, J. Huang, P. Russell, and J. St, Synthesis and dissociation of soliton molecules in parallel optical-soliton reactors, *Light: Sci. Appl.* **10**, 1 (2021).
- [37] M. Chernysheva, S. Sugavanam, and S. Turitsyn, Real-time observation of the optical sagnac effect in ultrafast bidirectional fibre lasers, *APL Photon.* **5**, 016104 (2020).
- [38] W. Zhang, L. Zhan, T. Xian, and L. Gao, Bidirectional dark-soliton fiber lasers for high-sensitivity gyroscopic application, *Opt. Lett.* **44**, 4008 (2019).
- [39] T. Ideguchi, T. Nakamura, Y. Kobayashi, and K. Goda, Kerr-lens mode-locked bidirectional dual-comb ring laser for broadband dual-comb spectroscopy, *Optica* **3**, 748 (2016).
- [40] B. Li, J. Xing, D. Kwon, Y. Xie, N. Prakash, J. Kim, and S.-W. Huang, Bidirectional mode-locked all-normal dispersion fiber laser, *Optica* **7**, 961 (2020).
- [41] Y. Yu, C. Kong, B. Li, J. Kang, Y.-X. Ren, Z.-C. Luo, and K. K. Wong, Behavioral similarity of dissipative solitons in an ultrafast fiber laser, *Opt. Lett.* **44**, 4813 (2019).
- [42] I. Kudelin, S. Sugavanam, and M. Chernysheva, Build-up dynamics in bidirectional soliton fiber lasers, *Photon. Res.* **8**, 776 (2020).
- [43] K. Goda and B. Jalali, Dispersive Fourier transformation for fast continuous single-shot measurements, *Nat. Photon.* **7**, 102 (2013).
- [44] Z. Wang, Q. Jiang, Z. Tang, and Z. Zhang, Complex pulsating dynamics of counter-propagating solitons in a bidirectional ultrafast fiber laser, *Opt. Express* **28**, 28209 (2020).
- [45] F. Krausz, M. E. Fermann, T. Brabec, P. F. Curley, M. Hofer, M. H. Ober, C. Spielmann, E. Wintner, and A. Schmidt, Femtosecond solid-state lasers, *IEEE J. Quantum Electron.* **28**, 2097 (1992).
- [46] J. Peng, M. Sorokina, S. Sugavanam, N. Tarasov, D. V. Churkin, S. K. Turitsyn, and H. Zeng, Real-time observation of dissipative soliton formation in nonlinear polarization rotation mode-locked fibre lasers, *Commun. Phys.* **1**, 1 (2018).
- [47] N. Wiener, Generalized harmonic analysis, *Acta Math.* **55**, 117 (1930).
- [48] A. Khintchine, Korrelationstheorie der stationären stochastischen prozesse, *Math. Ann.* **109**, 604 (1934).
- [49] L. Cohen, in *Proceedings of the 1998 IEEE International Conference on Acoustics, Speech and Signal Processing, ICASSP '98 (Cat. No. 98CH36181)*, Vol. 3 (IEEE, 1998), p. 1577.
- [50] I. Kudelin, S. Sugavanam, and M. Chernysheva, in *Nonlinear Optics and its Applications 2020*, Vol. 11358 (International Society for Optics and Photonics, 2020), p. 1135810.
- [51] J. Peng, N. Tarasov, S. Sugavanam, and D. Churkin, Rogue waves generation via nonlinear soliton collision in multiple-soliton state of a mode-locked fiber laser, *Opt. Express* **24**, 21256 (2016).
- [52] D. R. Solli, C. Ropers, P. Koonath, and B. Jalali, Optical rogue waves, *Nature* **450**, 1054 (2007).
- [53] Y. Bracamontes-Rodríguez, O. Pottiez, E. García-Sánchez, J. Lauterio-Cruz, H. Ibarra-Villalón, J. Hernandez-García, M. Bello-Jimenez, G. Beltrán-Pérez, B. Ibarra-Escamilla, and E. Kuzin, Dual noise-like pulse and soliton operation of a fiber ring cavity, *J. Opt.* **19**, 035502 (2017).
- [54] G. Herink, B. Jalali, C. Ropers, and D. R. Solli, Resolving the build-up of femtosecond mode-locking with single-shot spectroscopy at 90 MHz frame rate, *Nat. Photon.* **10**, 321 (2016).
- [55] X. Liu, D. Popa, and N. Akhmediev, Revealing the Transition Dynamics from Q Switching to Mode Locking in a Soliton Laser, *Phys. Rev. Lett.* **123**, 093901 (2019).
- [56] Y. Zhou, Y.-X. Ren, J. Shi, and K. K. Wong, Breathing dissipative soliton explosions in a bidirectional ultrafast fiber laser, *Photon. Res.* **8**, 1566 (2020).
- [57] K. Yang, T.-J. Li, X.-D. Li, J.-X. Chen, M. Liu, H. Cui, A.-P. Luo, W.-C. Xu, and Z.-C. Luo, Mutually induced soliton polarization instability in a bidirectional ultrafast fiber laser, *Opt. Lett.* **46**, 4848 (2021).
- [58] Y. Zhou, Y.-X. Ren, J. Shi, and K. K. Wong, Dynamics of breathing dissipative soliton pairs in a bidirectional ultrafast fiber laser, *Opt. Lett.* **47**, 1968 (2022).
- [59] Y. Zhou, Y.-X. Ren, J. Shi, and K. K. Wong, Breathing dissipative soliton molecule switching in a bidirectional mode-locked fiber laser, *Adv. Photon. Res.*, 2100318 (2022).
- [60] Q.-F. Yang, X. Yi, K. Y. Yang, and K. Vahala, Counter-propagating solitons in microresonators, *Nat. Photon.* **11**, 560 (2017).
- [61] E. Lucas, G. Lihachev, R. Bouchand, N. G. Pavlov, A. S. Raja, M. Karpov, M. L. Gorodetsky, and T. J. Kippenberg, Spatial multiplexing of soliton microcombs, *Nat. Photon.* **12**, 699 (2018).
- [62] T. Herr, V. Brasch, J. D. Jost, C. Y. Wang, N. M. Kondratiev, M. L. Gorodetsky, and T. J. Kippenberg, Temporal solitons in optical microresonators, *Nat. Photon.* **8**, 145 (2014).
- [63] T. J. Kippenberg, A. L. Gaeta, M. Lipson, and M. L. Gorodetsky, Dissipative Kerr solitons in optical microresonators, *Science* **361**, eaan8083 (2018).